Fluid Dynamic Analysis of Electrostatic Precipitators and Ionized Flows

Masaaki Okubo

Dept. of Mechanical Engineering
Osaka Prefecture University
phone: +81 72 254 9230
e-mail: mokubo@me.osakafu-u.ac.jp

***Abstract*— Fundamentals of electrostatic precipitator (EP) and three-dimensional electro-fluid dynamic flows are described. In recent years, EP research was thought to be a field that is released from academic researchers and was almost completely shifted to industry. However, due to the growing awareness of nanoparticle problems represented by recent $PM_{2.5}$ problems, EP characteristics of low pressure drop and high collection efficiency of nanoparticles are attracting attention as a substitute for filters, and application to automobiles is considered. In this paper, first, a system of basic equations governing electro-fluid dynamic ionized flows is presented. Based on the basic equations, results of the three-dimensional flow interaction for tuft or point corona for industrial EPs was reported using both laminar and turbulent flow models. In the results, the secondary flow distribution based on laminar flow model forms a pair of organized donut-shaped rings generated from every corona or tuft points, while a pair of rings is less organized for turbulent flow model. Next, because the temperature of the exhaust gas targeted by EP may sometimes reach 200°C or higher, systematically investigation of the influence of the exhaust gas temperature on the behavior of fine particles, the situation of secondary flow, and the reduced dust collection efficiency are shown and explained. Finally, other analysis results on EP are briefly reviewed. EP will become the core particulate (PM) removal technology of the future, and it can be expected to revitalize the research in the near future. We would like to perform detailed fluid dynamic analysis focusing on nanoparticle behavior**

I. INTRODUCTION

Electrostatic precipitators (EPs) have a long history, and their invention can be traced back to the beginning of the twentieth century. In recent years, almost all coal-fired power generation plants in Japan have been fully equipped with EPs, and they have certainly been a leading environmental tool in cleaning the country's skies. Their domestic rate of diffusion has been quite high, and they are now commonly used in a variety of industries (thermal power stations, steel manufacturing plants, paper manufacturing plants, cement factories, chemical plants, glass melting furnace, etc.). However, owing to the growing awareness of the problem of nanoparticles, typified by the recent $PM_{2.5}$ problem, EPs that are low in pressure drop and high in nanoparticle collection efficiency have taken the

spotlight in place of filters, and are being applied to indoor air cleaners, and are being explored for use in automobiles.

The author, compelled by the need for computer aided engineering (CAE) for various machines, have experience in analyzing the flow (two-phase flow) of fluids (liquids, gas, plasma) containing particles (or vapor bubbles and liquid droplets) and the motion of particles under the action of electromagnetic forces [1]. Presently, analytical methods and fundamental equations differ depending upon on differences in subjects, and they require familiarization with simulation techniques peculiar to each field, as well as the building of computer programs. In addition, in order to pursue experiments and simulations in parallel within a limited time, it is wise to use recently developed simulation software or solvers. However, even in these cases, adequate understanding of fundamental equations, initial conditions, boundary conditions, and analytical methods is necessary.

We previously explained the fundamentals of EP analysis in previous paper [2]. Here, we shall utilize three-dimensional two-phase flow in an EP as the subject, assume analysis using commercial simulation software, and explain a system of basic equations and solutions for electric fluid flow and particle motion. In the latter half, we shall newly introduce several simulation results using this as their foundation.

II. System of Basic Equations [1]–[9]

Three-dimensional two-phase flow of an EP may be analyzed through simultaneous numerical analysis using three systems of equations: Maxwell's equations for electromagnetic fields, a system of fluid (gas) flow momentum equations, and a system of collected particle momentum equations. Of these, space potential needs to be found in a state of ions or other charged particles (electrical charge) distributed in space, thus the equation for the potential is essentially Poisson's equation. In addition, the equation for flow fields is the Navier-Stokes equation, which accounts for electrostatic forces. Particle and fluid flow has relative velocity, and forms a two-phase flow. For the momentum equation for particles, we had two techniques. When we considered particle phases to be a continuum (fluid), we used the Euler method, which is treated as a partial differential equation. When we considered the force applied to a single particle, we utilized the Lagrangian method, which is treated as a system of ordinary differential equations. However, in practical analysis of EPs, the easily understood Lagrangian method is often used, where the trajectories of individual test particles in a machine are found. Normally, that act on particles from surrounding fluid is considered; however, the impact of particles themselves and the reaction force exerted by particles on fluid is assumed to be small in effect and is not considered. It should be noted that the physical variable of the electric field and flow field equations is the size of the field as a function of static coordinates (globally fixed coordinate system), while the physical variable of the particles is different, and is a point acting as the physical quantity held by a single moving particle. The above system of basic equations is shown below.

A. System of Basic Equations for Electric Fields

The Maxwell's equations (electromagnetic field equations) regularly used in EP analysis are equations for electric flux density $\boldsymbol{D}$ and current density $\boldsymbol{J}$.

$$\nabla \cdot \boldsymbol{D} = \rho_e, \quad \boldsymbol{D} = \varepsilon_r \varepsilon_0 \boldsymbol{E} \tag{1), (2)}$$

$$\frac{\partial \rho_e}{\partial t} + \nabla \cdot \boldsymbol{J} = 0 \tag{3}$$

$$\boldsymbol{J} = \rho_e \boldsymbol{u} + \sigma \boldsymbol{E} = \rho_e (\boldsymbol{u} + b\boldsymbol{E}) \approx \rho_e b \boldsymbol{E} \tag{4}$$

where ρ_e is the volume charge density, ε_r is the relative dielectric constant, ε_o is the dieletric constant of vacuum, $\boldsymbol{u}$ is the fluid velocity, and b is the ion mobility. The value of b varies depending on the type of gas and whether ions are positive or negative, but can be regarded as a constant at constant temperature. When negative ions in the air are the target particles, $b = 2.0 \times 10^{-4}$ m^2/ (Vs) (20°C) in reference [3], $b = 1.51 \times 10^{-4}$ m^2/ (Vs) (0°C) in reference [8], and $b = 2.5 \times 10^{-4}$ m^2/ (Vs) (0°C) in literature [9]. In addition, ion velocity may be assumed to be large compared to u, and in that case an approximation of equation (4) holds. Potential (voltage) ϕ may be introduced by $\boldsymbol{E} = -\nabla\phi$, and Poisson's equation can be obtained from equations (1) and (2).

$$\nabla \cdot (\varepsilon_r \varepsilon_0 \nabla \phi) = -\rho_e \tag{5}$$

In addition, when equation (4) is substituted into equation (3), and the spatial discharge ρ_e is assumed to be stationary, equation (6) is obtained. Furthermore, when the left side of equation (6) is expanded, and equation (5) is considered, equation (7) is obtained.

$$\nabla \cdot (\rho_e b \nabla \phi) = 0 \text{ or } \varepsilon_0 \nabla \rho_e \cdot \nabla \phi = \rho_e^2 \tag{6), (7)}$$

By solving equation (5) and equation (6), or equation (7), under the proper boundary conditions, the distribution of $\boldsymbol{E}$, ϕ, and ρ_e is determined.

B. Basicl Equations of Thermal Fluid

Basic equations of fluid (gas) flow within a machine are a continuity equation (mass conservation law) and a momentum equation (momentum conservation law), and they are generally formulated as follows.

$$\frac{\partial \rho}{\partial t} + \nabla \cdot (\rho \boldsymbol{u}) = 0 \tag{8}$$

$$\frac{\partial (\rho \boldsymbol{u})}{\partial t} + \nabla \cdot (\rho \boldsymbol{u}\boldsymbol{u}) = -\nabla p + \nabla \cdot (\mu \nabla \boldsymbol{u}) + \frac{1}{3}\mu \nabla (\nabla \cdot \boldsymbol{u}) + \rho_e \boldsymbol{E} \tag{9}$$

Here, ρ is fluid density, t is time, p is pressure, and μ is fluid viscosity coefficient. We consider electrostatic force as the volume force acting on fluid, which is a source of secondary flow due to ion wind. The energy equation for determining fluid temperature T (equation of state and law of the conservation of energy) is as follows.

$$p = \rho R T \tag{10}$$

$$C_{\mathrm{p}}\left[\frac{\partial(\rho T)}{\partial t}+\nabla\cdot(\rho \boldsymbol{u} T)\right]=\nabla\cdot(\lambda\nabla T)+\psi_{\mathrm{D}}+S_{\mathrm{c}} \tag{11}$$

where source terms include R, the gas constant; T, the absolute temperature; C_{p}, the specific heat at constant pressure; λ, the thermal conductivity; ψ_{D}, the dissipative energy loss; and S_{c}, the heat for the chemical reaction. The distribution of $\boldsymbol{E}$, ϕ, and ρ_{e} are determined from equations (5) to (7), and by solving equations (8) to (11) from this distribution, flow field u and temperature T are found.

C. Particle Electric Charge Equations

The key factor for an accurate simulation of EP collection efficiency is the estimates of the amount of particle electric charge. If particles larger than 1 μm in diameter are the target particles, then the so-called electric charge is dominant. The mechanism of this is ions moving along an electric field colliding with particles, adhering to them, and then electrically charging them. The amount of electric charge gradually increases, achieving saturation charge $q_{\max}$. The electric charging process may be expressed by the relaxation equation below [2].

$$\frac{\mathrm{d}q}{\mathrm{d}t}=\frac{1}{\tau q_{\max}}(q_{\max}-q)^2 \tag{12}$$

$$q_{\max}=\frac{3\pi\varepsilon_0\varepsilon_{\mathrm{r}}|\boldsymbol{E}|d_{\mathrm{p}}^2}{\varepsilon_{\mathrm{r}}+2} \tag{13}$$

where q is the amount of particle electric charge, and $\tau = 4\varepsilon_0/(\rho_{\mathrm{e}} b)$ is the relaxation time until the particle electric charge has reached 50% saturation. Because this is extremely small at $\tau = 10^{-3}$ s, q may be a particle immediately reaching saturation upon entering an EP.

If nanoparticles of approximately $d_{\mathrm{p}} < 100$ nm are the target particles, then diffusion discharge is dominant. The change over time of the amount of particle charge is expressed by the following equations [9].

$$q(t)=q^*\ln\left(1+\frac{t}{\tau^*}\right) \tag{14}$$

$$q^*=\frac{2\pi\varepsilon_0 d_{\mathrm{p}}^2 kT}{e} \tag{15}$$

where k is Boltzmann's constant, and e is the elementary charge. Theoretically, the amount of saturation charge $q_{\max}$ is not present in equation (14), however, $q = 6.2q^*$ at $t = 500\tau^*$ are used as a value for $q_{\max}$ [9].

D. Particle Momentum Equation

A momentum equation for simulating the motion of one test particle may be written as follows, according to Lagrangian method.

$$m_{\mathrm{p}} \frac{d\boldsymbol{u}_{\mathrm{p}}}{dt} = \frac{C_{\mathrm{D}}}{C_{\mathrm{C}}} \rho \left(\boldsymbol{u} - \boldsymbol{u}_{\mathrm{p}}\right) \left|\boldsymbol{u} - \boldsymbol{u}_{\mathrm{p}}\right| \frac{A_{\mathrm{p}}}{2} + m_{\mathrm{p}} \boldsymbol{g} + q\boldsymbol{E} + \boldsymbol{F}_{\mathrm{Ba}} + \boldsymbol{F}_{\mathrm{Saff}} + \boldsymbol{F}_{p} + \boldsymbol{F}_{\mathrm{Br}} \tag{16}$$

where m_{p} is the mass of a single particle, $\boldsymbol{u}_{\mathrm{p}}$ is the particle velocity vector, C_{D} is the drag coefficient, C_{C} is Cunningham's correction factor, ρ is the surrounding fluid density, A_{p} (if spherical, $=\pi d_{\mathrm{p}}^{\,2}/4$) is the particle projection area, and $\boldsymbol{g}$ is the gravity vector. On the right side of equation (16), we have $\boldsymbol{F}_{\mathrm{Ba}}$, the Basset force; $\boldsymbol{F}_{\mathrm{Saff}}$, the Saffmann lift force; $\boldsymbol{F}_{\mathrm{p}}$, the force due to pressure gradient (including buoyancy); and $\boldsymbol{F}_{\mathrm{Br}}$, the force due to Brownian diffusion for fluid Stokes resistance, gravity, electrostatic force, and unsteady drag force. Furthermore, the inertial force due to the virtual mass is small in solid-gas two-phase flows, thus it generally may be ignored.

On the right side of equation (16), the influence of Stokes' resistance, gravity, and electrostatic force is generally significant. Drag is influenced not only by particle shape and direction but also by particle Reynolds number, turbulence level and other factors. Nanoparticles that are small in particle size have sizes approximately the same as the mean free path of gas fluid molecules, thus particle slip is produced, and Stokes' resistance needs to be corrected. As shown in equation (16), corrections may be applied by dividing C_{D} by C_{C} (>1). Furthermore, $\boldsymbol{F}_{\mathrm{Ba}}$, $\boldsymbol{F}_{\mathrm{Saff}}$, $\boldsymbol{F}_{\mathrm{p}}$, and $\boldsymbol{F}_{\mathrm{Br}}$ ought to be properly considered in precise calculation.

E. Boundary Conditions

The boundary conditions for solving the aforementioned fundamental equations must consider two types of boundary conditions: (a) thermo-fluid dynamic boundary conditions, such as a zero velocity on wall surfaces, constant velocity gradient, constant temperature, constant heat flux, and free in and outflow conditions; and (b) electromagnetic field boundary conditions, which are imposed when the potential ϕ or another value for a physical quantity is conferred on a boundary for electro-fluid dynamics, or when there is a boundary surface consisting of two mediums with different conductivity values within a system, wherein the normal component of current density $\boldsymbol{J}$ is continuous (e.g., the tangential component of electric field $\boldsymbol{E}$).

Boundary conditions should be given in accordance with actual systems, and are difficult to describe in a unified manner. We will provide an outline of them on an individual basis in analytical cases below.

F. Analytical Procedure

We numerically solve the equations governing electro-hydrodynamics described above by differential coupling, and then make calculations including electric fields, electrical charge fields, velocity fields, temperature fields, and particle trajectories. Electric fields, electrical charge fields, velocity fields and temperature fields comprise a system of simultaneous partial differential equations; however, electric fields and electrical charge fields may be determined independently, and they pose relatively easy problems for coupling computational hydrodynamics. In addition, in EP analysis, it is often assumed that flow

fields are stationary, temperature is constant (with no consideration of changes in gas temperature), and energy equations (10) and (11) are not analyzed. In addition, if flow velocity or Reynolds number becomes larger, and the main flow becomes turbulent, then if the computational grid near the flow path is not extremely fine, then an accurate solution will not be achievable with direct simulation. Therefore, we interpolate velocity distribution near a wall with a wall function or something similar, and then use turbulence models such as k–ε model, etc. to consider turbulent viscosity. In addition, when the flow reaches high speed close to the speed of sound, the influence of incompressible is considered therefore, normally, analysis is done with incompressible models of constant fluid density.

For two-phase flow calculation, CFD-ACE+ [1], FLUENT [5], [6], and STAR-CD [7], [8], for example, are well-known solvers. If these are used, the simulations proceed with various conditions stipulated in the software for solvers.

III. Examples of Analysis

Thereafter, using the above system of basic equations, we shall introduce a study in which an EP was implemented; in other words, an application example. For the sake of calculation cost and other factors, approximation is performed in each analysis, where only a few terms in the aforementioned fundamental equations are considered; however, terms that are of negligible influence are ignored. Readers interested in more detailed explanations should be motivated by this text to consult the relevant papers.

A. Three-Dimensional Analysis of Ion Wind Secondary Flow Within Tuft/Point Corona Discharge EP

1) Use of Point Type Discharge Electrode, and Electric Field, Electrical Charge, and Flow Field Calculations

In the years since the implementation of EP, wire (piano wire) discharge electrodes and flat plate collecting electrodes have been adopted; however, dust adheres to discharge electrodes, often leading to decreased collection performance problems because of insufficient current or discharge electrode disconnection accidents. In recent years, EPs have increased owing to an increase in the amount of processing gas; furthermore, there is an increased demand for improved performance and machine reliability, and a general adoption of point (projected) type discharge electrodes (tuft/point corona discharge wire) in which current easily flows. In particular, with submicron high-density particle collection in the exhaust gas of high sulfur-oil-fueled boilers, long projected type discharge electrodes are essential for dealing with decreased performance due to increased dust collection spatial discharge effects.

We shall introduce the results of analyzing EP flow within such EP [3], [4]. Flow is the superimposition of a main flow and secondary flow, which is called ion wind in static electric fields. First, we analyze equations (5) and (7) by successive relaxation method using finite differential method, and obtained the distribution of E, ϕ, and ρ_e. Specifically, we followed the procedure below. We used Cooperman's solution (a solution to Laplace equation)[(2)] as an initial condition. We differentiated the obtained potential ϕ, and determined the initial values of the electric field intensity E_x, E_y and E_z in the main flow direction x, direction perpendicular to the collecting plate electrode y, and direction parallel to the collecting plate electrode z. Using these initial values and current density set values, we

obtain values for spatial discharge density near tuft/point corona by Ohm's law equation (4). Furthermore, we used the obtained values for spatial discharge density, and potential (voltage) is calculated from Poisson's equation (5). When this is done, calculations are repeated until the difference between the newest value of voltage and voltage value one before at each lattice point is within 0.01%. Finally, if we compare current density values and set values, and the difference does not match within 0.01%, calculation is repeated. Assuming a constant flow field temperature, only the continuity equation (8) and the momentum equation (9) are analyzed. We use a k–ε model as a turbulence model.

2) Calculation Results for Ion Wind without Main Flow

Fig. 1 shows the results of analyzing a flow field excited by ion wind without main flow. The line in the figure represents the flow line, and the differences in color represent differences in positions in the y-axis direction in the dust collection space. In addition, in **Fig. 1** (**a**) and (**b**), flow in a x-y plane including a point corona is symmetrical, thus only the top flow field is displayed. Donut-shaped ring flow originating from a point discharge electrode, blowing out radially in the collecting electrode direction and gas flow direction, and also returning in the discharge electrode direction occurs in the dust collection space between point discharge electrodes. **Fig. 2** (omitted in this paper) shows a schematic depiction of the flow regime.

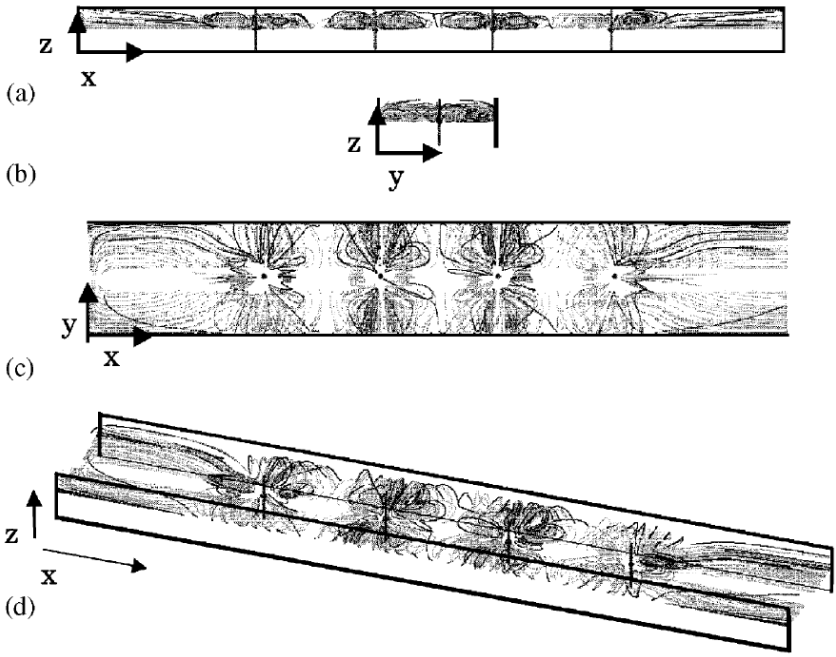

Fig. 1. Flow in the collecting region without main stream, (a) x - z cross - sectional view, (b) y - z cross - sectional view, (c) x - y cross - sectional view, (d) 30 - degree inclined view (U = 0.0 m/s, $N_{ehd} = \infty$) [3]

Fig. 2 (omitted in this paper) Schematics of three dimensional secondary flow form near the point discharge electrode

3) Calculation Results for Ion Wind with Main Flow.

Fig. 3 shows the results of analyzing a flow field with a main flow present, as well as nonlinear interaction with ion wind. As main flow velocity becomes larger, ring flow is suppressed as shown in **Fig. 2**, moves in the downstream direction, and overall flow starts to rotate, and three-dimensional spiral flow is formed. Then, when main flow velocity is approximately 0.5 m/s, three-dimensional spiral flow is suppressed as shown in **Fig. 3**, becomes diffused, and turns into mixed flow in the outlet. It is believed that such flow may be formed in an actual EP dust collection space.

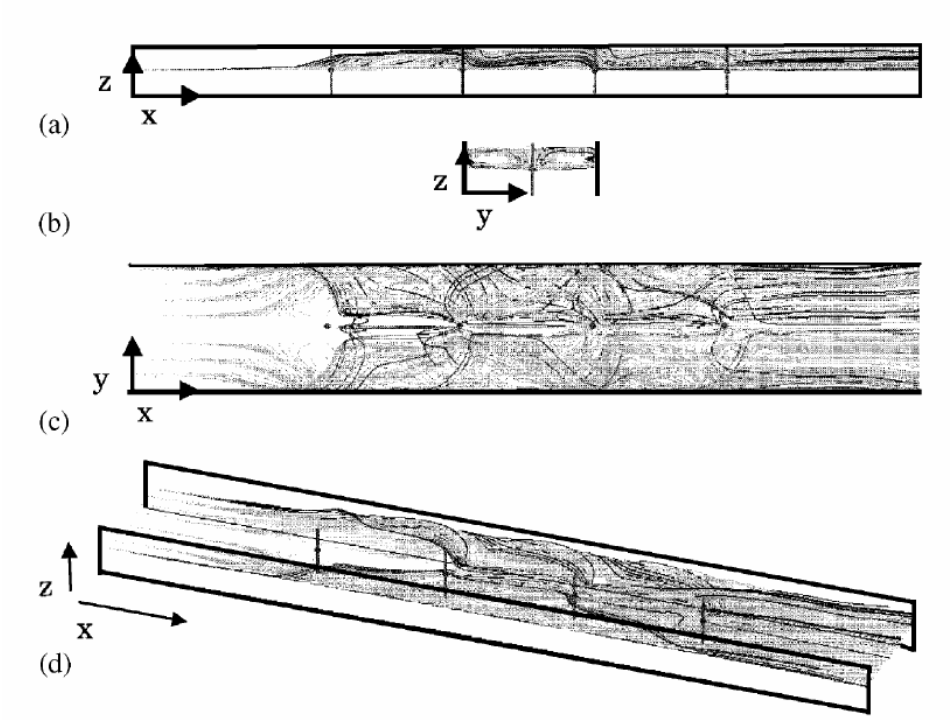

Fig. 3. Turbulent flow in the collecting region, (a) x - z cross - sectional view, (b) y - z cross - sectional view, (c) x - y cross - sectional view, (d) 30 - degree inclined view (U = 0.5 m/s, N_{ehd} = 0.477) [3]

The following EHD number N_{ehd} is assumed to be a dimensionless number representing the influence of the secondary flow (ion wind) flow velocity u_e upon the mainstream of gas U.

$$N_{ehd} = u_e / U, \quad u_e = \sqrt{J_p d /(b\rho)} \tag{17}$$

where U: main flow typical velocity, J_p: collecting plate current density immediately below point corona, d: electrode interval between discharge electrode and collecting electrode, ρ:

fluid density, and b is the aforementioned ion mobility. In the results in **Fig. 3**, we assume u_e = 0.237 m/s (J_p = 0.12 mA/m^2, d = 0.114 m, b = 2.0 × 10^{-4} m^2/ (Vs), and ρ = 1.205 kg/m^3 (20°C)) and U = 0.5 m/s, and therefore N_{ehd} = 0.477. However, in actual dry type EP for coal fired boilers, J_p = 0.2–0.3 mA/m^2, d = 0.15 m, and U = 1.0 m/s are common values, thus N_{ehd} = 0.432, and although current density and velocity values are different, the results in **Fig. 3** may be said to be ones in which similar flow is calculated for an actual machine. Furthermore, according to Adachi et al. [10], when EHD number exceeds 2, ion wind becomes larger, and flow is largely turbulent. However, under general operating conditions for this type of EP, EHD number is at most approximately equal to 1, and it is believed that ion wind does not have much influence.

B. Effects of Three-Dimensional Secondary Flow

Regarding the influence of the secondary flow in EHD, its effect is also quantitatively simulated in a study [5] by Western University in Canada. The software used is FLUENT. The state of secondary flow generated in **Fig. 4** (omitted in this paper) is cited in reference [5]. Simulation results are from changing flow velocity to an inlet to 0 to 1.0 m/s. If main flow velocity u = 0 m/s in the figure (**Fig. 4a**), the four fully-developed largely symmetrical large vortices are observed, and the intersection of the boundaries of the four vortices is the location of discharge electrode wire. If the inlet flow velocity is raised, and u = 0.1 m/s (**Fig. 4b**), the two wire upstream vortices become somewhat smaller because of the flow, while the two downstream vortices have a tendency to expand downstream. If flow velocity is raised to u = 0.2 m/s (**Fig. 4c**), then this tendency becomes more pronounced. From the nonlinearity of the NS equation, this is a convection phenomenon which cannot be simply explained from a mere superposition of main flow and ion wind, which is an interesting phenomenon from the viewpoint of fluid dynamics. When flow velocity is raised from u = 0.4 m/s to u = 0.5 m/s (**Fig. 4d** and **Fig. 4e**), two vortices appear only near the collecting electrode, and themselves become quite small. When inlet flow velocity increases to u = 1.0 m/s (**Fig. 4f**), the effect of EHDS secondary flow may be largely ignored, and a uniform main flow pattern comes to occupy the middle of the flow path.

Under conditions with an EHD flow vortex present under the condition u = 0.5 m/s shown in **Fig. 4e**, compared to when there is no vortex present, a 2% improvement in collection efficiency for particles of 1 μm from 28.5% to 30.5% is obtained. It is believed that this is due to the effect of particles pressing against the electrode plate. However, reported hardly any improvement in collection efficiency for particles of larger sizes 5, 10 and 50 μm is seen.

Fig. 4. (omitted in this paper) Calculation result of streamline of secondary flow among collecting electrodes for various inlet flow velocities affecting particle collection. The figure is reprinted from reference [5]

C. Effect of Gas temperature on EP collection Efficiency

The temperature of exhaust gas targeted by EPs sometimes reaches 200°C or higher, and few studies have been reported systematically examining the influence of such high exhaust gas temperature on particle behavior, secondary flow situations, and decreased collection efficiency. Here, we introduce the results of examining this through numerical simulation [6].

As exhaust gas reaches high temperatures, ion wind strength increases, and the secondary flow becomes pronounced. This is mainly due to the mechanism below. Ion electric charge density (C/m^3) increases overall as temperature rises and, at high temperatures, the viscosity coefficient of gas becomes larger; hence, there is a stronger tendency for the force experienced by the particles in the flow and electric fields (drag force and electrostatic force) to become larger and move along the flow fields. According to the momentum conservation law of gas flow, the influence of secondary flow may be neglected with low mass flow rates or low inlet flow velocity. However, the influence of secondary flow on collection becomes larger the smaller the size of the targeted particles, at which point the influence upon collection efficiency becomes pronounced. Particle trajectories, when particles are collected between electrodes, are precisely simulated in calculation results for whether or not there is secondary flow, and results are reported in which secondary flow has a greater influence when gas temperatures are high, particle densities are large, and particle sizes are small. In addition, there are two types of charge principles for particles: one for the electric charge and one for diffusion discharge. The former weakens as temperature rises, while the latter becomes stronger. Accordingly, it is believed that collection efficiency increases for particles that are small particle size and large in diffusion discharge influence.

The other results may be presented in the lecture.

IV. Conclusion

We explained the fundamental equations for analyzing fluid flow and particle motion, analytical methods, and the results of analyzing fundamental equations, regarding three-dimensional two-phase fluid simulation of an electrostatic precipitator (EP). EPs will become the main particulate matter (PM) removal technology in the future. EPs are being explored for future use because of their superior nanoparticle collection with little ventilation pressure drop. This is not only for large-scale EPs in thermal power stations but also, for example, for PM removal equipment in diesel automobiles currently using ceramic filters. Studies on the use of marine diesel EPs are also progressing. Nonetheless, the problem of re-scattering of low resistivity fine particles cannot be said to be completely solved. However, countermeasures such as hole type EP [7], [8] have reached their practical application stage. Here, hole type EP refers to those devised for the purpose of preventing re-scattering from collecting electrode plates for particles that are low in electrical resistivity ($<10^4\ \Omega$ cm), such as diesel engine exhaust particles, which enable prevention of re-scattering by having collected particles brought from holes into pockets on the outer circumference of ground electrodes.

EP simulation is a field of study at the boundary of electrical and mechanical engineering, and has traditionally not been dealt with by machine researchers. The behavior of electric charge nanoparticles and electric fluid secondary flow is an extremely interesting phenomenon from a fluid engineering viewpoint, and it is expected that it will be addressed in the mechanical engineering field in future. In addition, it may be applied to the analysis of environmental plasma technology to form non-thermal plasma by applying unsteady alternating current (AC) or pulse high voltage between electrodes, not only regarding particle collection but also regarding the decompositions of nitrogen oxide (NO_x) [11] and carbon dioxide (CO_2) [12]. We would be pleased if this paper assisted those engaged in the numerical simulation of EPs.

ACKNOWLEDGMENT

We would like to thank postdoctoral researcher Hidekatsu Fujishima of Osaka Prefecture University for his assistance in writing this paper. This paper is a conference paper for proc. 2018 Electrostatics Joint Conference and provide a summary of our research. A complete report will be submitted to J. Electrostatics.

REFERENCES

[1] S. Kambara, M. Okubo, et al (joint authorship), "Atmospheric pressure plasma reaction engineering handbook - Fundamentals of reaction process and actual simulation," NTS, Inc., pp. 59–85, 2013.

[2] M. Okubo and H. Fujishima, "Fundamentals of electrostatic precipitator two - phase flow numerical simulation," *Journal of the Institute of Electrostatics Japan*, 40 (4), pp. 162–167, 2016 (in Japanese).

[3] T. Yamamoto, Y. Morita, H. Fujishima, and M. Okubo, "Three-dimensional EHD simulation for point corona electrostatic precipitator based on laminar and turbulent models," *J. Electrostat*., 64, pp. 628–633, 2006.

[4] T. Yamamoto, M. Okuda, and M. Okubo, "Three-dimensional ionic wind and electrohydrodynamics of tuft/point corona electrostatic precipitator," *IEEE Trans. Ind. Applicat.*, 39 (6), pp. 1602–1607, 2003.

[5] N. Farnoosh, K. Adamiak, and G. S. P. Castle, "3-D numerical analysis of EHD turbulent flow and mono - disperse charged particle transport and collection in wire – plate," ESP, *J. Electrostat*., 68, pp. 513–522, 2010.

[6] Y. Li, C. Zheng, K. Luo, X. Gao, J. Fan, and K. Cen, "CFD simulation of high - temperature effect on EHD characteristics in a wire - plate electrostatic precipitator," *Chinese J. Chem. Eng.*, 23, pp. 633–640, 2015.

[7] K. Kawakami, A. Zukeran, K. Yasumoto, T. Inui, Y. Enami, Y. Ehara, and T. Yamamoto, "Re - scattered particle trajectory simulation with a double cylinder type electrostatic precipitator," *Journal of the Japan Institute of Marine Engineering*, 46 (5), pp. 111–117, 2011 (in Japanese).

[8] H. Kawakami, A. Zukeran, K. Yasumoto, T. Inui, Y. Ehara, and T. Yamamoto, "Numerical simulation of three - dimensional particle migration and electrohydrodynamics of double cylinder electrostatic precipitator," *Int. J. Plasma Env. Sci. & Tech.*, 6 (2), pp. 104–110, 2012.

[9] Edited by The Institute of Electrostatics Japan, Electrostatics Handbook, Ohmsha, Ltd., p. 47, p. 1204, p. 1125, 1985 (in Japanese).

[10] T. Adachi and T. Okubo, "Ion wind generated by corona discharge," *Journal of the Institute of Electrostatics Japan*, 11 (4), pp. 246–254, 1987 (in Japanese).

[11] T. Kuwahara, K. Yoshida, T. Kuroki, K. Hanamoto, K. Sato, and M. Okubo, "Pilot-scale after-treatment using nonthermal plasma reduction of adsorbed NO_x in marine diesel–engine exhaust gas," *Plasma Chem. Plasma Process*., 34 (1), pp. 65 – 81, 2014.

[12] K. Nakajima, K. Takahashi, M. Tanaka, T. Kuroki, and M. Okubo, "CO_2 reduction using adsorption followed by nonthermal plasma treatment, *J. Phys. Conf. Series*, 646 (1), 012056, total 4 pages, 2015.